DOI: 10.1002/ejic.200801094

First Row Transition Metal Aminopyridinates – the Missing Complexes

Germund Glatz,[a] Serhiy Demeshko,[b] Günter Motz,[c] and Rhett Kempe*[a]

Keywords: N ligands / Cobalt / Iron / Manganese / Scandium / Zinc

Lithiated 4-methyl-2-[(trimethylsilyl)amino]pyridine ($Ap^{TMS}H$) undergoes a salt metathesis reaction with $[ScCl_3(thf)_3]$ and $FeCl_3$, at low temperature in thf, to yield the homoleptic complexes $[Sc(Ap^{TMS})_3]$ (**1**) and $[Fe(Ap^{TMS})_3]$ (**2**). An analogous reaction with $MnCl_2$, $CoCl_2$ and $FeCl_2$ using two equivalents of 4-*tert*-butylpyridine (*t*BuPy) as additional donor ligand affords the structurally analogous *cis* complexes $[Mn(Ap^{TMS})_2(tBuPy)_2]$ (**3**), $[Co(Ap^{TMS})_2(tBuPy)_2]$ (**4**) and $[Fe(Ap^{TMS})_2(tBuPy)_2]$ (**5**). If $FeCl_2$ is used without *t*BuPy, the highly symmetric trinuclear complex $[Fe_3(Ap^{TMS})_6Li_2O]$ (**6**) is obtained. Furthermore, the use of $ZnCl_2$ in a reaction with lithiated $Ap^{TMS}H$ yields the dimeric complex $[Zn_2(Ap^{TMS})_4]$ (**7**) in which two Ap^{TMS} ligands bridge the two metals. All complexes have been characterised by X-ray crystal structure analysis. To the best of our knowledge, complexes **1** and **2** and **5** are the first scandium and iron aminopyridinates, respectively, and complex **3** is the first manganese aminopyridinate complex which contains no additional anionic ligand. Complexes **4** and **7** are rare examples of cobalt and zinc aminopyridinates. This study proves that aminopyridinato ligands are highly universal ligands since they are able to stabilize early and late transition metals. Aminopyridinates of every first row transition metal are now available. The magnetic properties of all paramagnetic complexes were investigated. All complexes are high-spin complexes and the trinuclear iron complex **6** exhibits a weak antiferromagnetic coupling.

Introduction

Aminopyridinates of the first row transition metals have been investigated for years.[1–3] Such complexes are mostly known for early transition metals like titanium, vanadium and chromium,[4–10] and only a few examples are known for the later first row transition metals like cobalt,[11] nickel,[12] copper[13,14] and zinc.[15] To the best of our knowledge, there are no known examples of aminopyridinate complexes of scandium and iron. A variety of related complexes are known for manganese,[16] cobalt,[17,18] nickel,[19] copper[20,21] and zinc,[22,23] but the ligands used are better described as pyridine-substituted sulfonamides rather than aminopyridinates because only the pyridine nitrogen of the ligand binds to the metal atom in many cases. Additionally, some complexes containing residual anionic non-aminopyridinate fragments such as a cyclopentadienido fragment[24,25] (manganese), ethyl,[13] methyl[15] or μ^4-oxo group[26] (zinc) are known. We decided to investigate whether it is possible to isolate stable aminopyridinate complexes of all first row transition metals using deprotonated, silyl-substituted aminopyridines since we plan to use such complexes to prepare metal-containing SiCN ceramics and would prefer not to introduce elements (beside the wanted metal) which are not part of the ceramic precursor. Herein we report on the synthesis and structural characterisation of Ap^{TMS} complexes of scandium, manganese, iron, cobalt and zinc and some aspects of the magnetic behaviour of the paramagnetic complexes.

Results and Discussion

4-Methyl-2-[(trimethylsilyl)amino]pyridine ($Ap^{TMS}H$) was obtained following a published procedure.[27] The product was isolated in very good yields and purified by distillation. $[ScCl_3(thf)_3]$ was synthesised according to a literature procedure.[28] The synthesis of all complexes presented here is shown in Scheme 1. A mixture of three equivalents of $Ap^{TMS}H$ and three equivalents of *n*BuLi in Et_2O was treated with one equivalent of $[ScCl_3(thf)_3]$ or $FeCl_3$ in thf. After workup, $[Sc(Ap^{TMS})_3]$ (**1**) was obtained as a white powder in moderate yields. In the case of iron, a deep purple precipitate of $[Fe(Ap^{TMS})_3]$ (**2**) was obtained in moderate yields. Crystalline **1** and **2** could be obtained by concentration of the mother liquor followed by storage at –30 °C. The ^1H NMR spectrum of **1** exhibits singlets at δ = 0.37 and 1.76 ppm for the trimethylsilyl group and the methyl group attached to the pyridine ring, respectively.

Additional signals at δ = 5.82, 6.33 and 7.55 ppm belong to the three aromatic protons. The ^{29}Si NMR spectrum shows one signal at δ = –5.62 ppm. The X-ray crystal struc-

[a] Lehrstuhl für Anorganische Chemie II, Universität Bayreuth, 95440 Bayreuth, Germany
E-mail: kempe@uni-bayreuth.de
[b] Institut für Anorganische Chemie, Georg-August-Universität Göttingen,
Tammannstraße 4, 37077 Göttingen, Germany
[c] Lehrstuhl Keramische Werkstoffe, Universität Bayreuth, 95440 Bayreuth, Germany

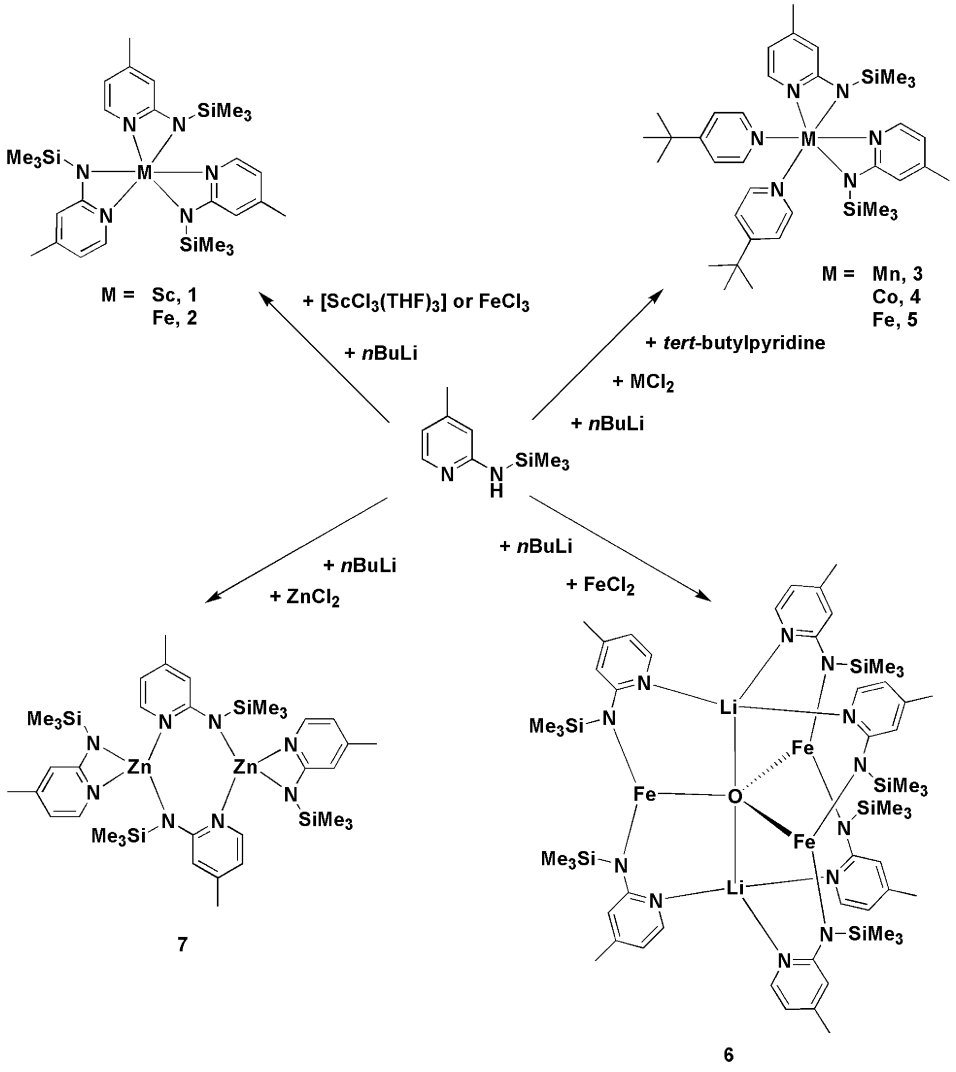

Scheme 1. Synthesis of **1**–**7**.

ture analyses of complexes **1** and **2** show that they are monomeric in the solid state (Figures 1 and 2, respectively), with the metal coordinated by three ligands in a distorted octahedral fashion. All ligands are η^2-coordinating. The $N_{pyridine}$–Sc bond lengths vary from 2.220(5) (N3–Sc1) to 2.245(4) Å (N5–Sc1) and the N_{amido}–Sc bond lengths from 2.169(4) (N4–Sc1) to 2.182(4) Å (N6–Sc1), with just a small difference between the two different nitrogen donor types.[29] The Sc–N distances in complex **1** lie in between those for a pure Sc–N_{amido} bond (2.000 Å)[30] and a pure Sc–$N_{pyridine}$ bond (2.309 Å).[31] This can be understood as a "mixture" of both amidopyridine and aminopyridinate binding modes[29] and a significant delocalisation of the anionic function of the ligand at the N_{amido} atom. The N–Sc–N bond angles vary from 61.81° (N6–Sc1–N5) to 62.31° (N2–Sc1–N1) and reveal the highly strained binding mode of the aminopyridinate ligands.

In the case of iron, the $N_{pyridine}$–Fe bond lengths range from 2.147(3) (N3–Fe1) to 2.191(3) Å (N5–Fe1) and the N_{amido}–Fe distances from 2.037(3) (N6–Fe1) to 2.054(3) Å

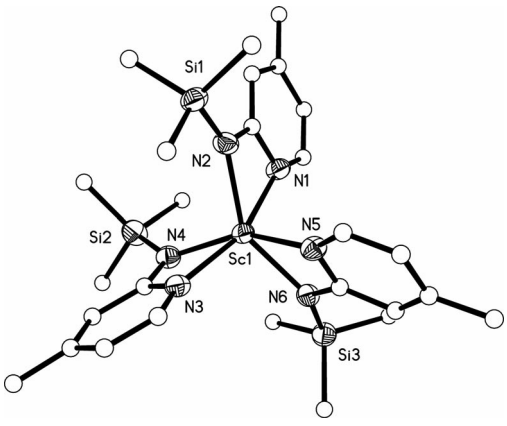

Figure 1. Molecular structure of **1** (ORTEP view; for clarity, only non-carbon atoms are drawn as 50% probability ellipsoids). Selected bond lengths [Å] and angles [°]: Sc1–N1 2.225(4), Sc1–N2 2.174(4), Sc1–N3 2.220(5), Sc1–N4 2.169(4), Sc1–N5 2.245(4), Sc1–N6 2.182(4); N1–Sc1–N2 62.31(15), N3–Sc1–N4 62.22(16), N5–Sc1–N6 61.81(15).

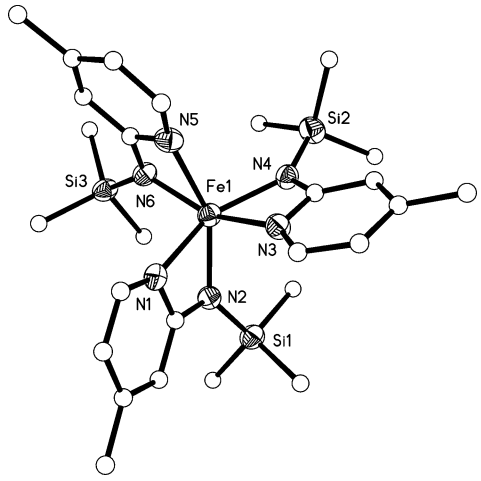

Figure 2. Molecular structure of **2** (ORTEP view; for clarity, only non-carbon atoms are drawn as 50% probability ellipsoids). Selected bond lengths [Å] and angles [°]: Fe1–N1 2.166(3), Fe1–N2 2.042(3), Fe1–N3 2.147(3), Fe1–N4 2.054(3), Fe1–N5 2.191(3), Fe1–N6 2.037(3); N1–Fe1–N2 64.06(10), N3–Fe1–N4 64.14(10), N5–Fe1–N6 63.74(10).

(N4–Fe1). A pure iron(III)–N_{amido} bond is about 1.918 Å,[32] whereas iron(III)–pyridine distances vary from 1.984[33] to 2.274 Å[34] and depend on the temperature and spin state.[33] The N–Fe distances in complex **2** are therefore indicative of a dominant amidopyridine binding mode. The Fe–N bond angles range from 63.74° (N5–Fe1–N6) to 64.14° (N3–Fe1–N4).

The N–M–N angles of the homoleptic trivalent metal aminopyridinates (Sc^{3+}, Fe^{3+}, Ti^{3+},[4] Cr^{3+}[4]) decrease with increasing effective ionic radius of the metal (Table 1). This can be explained geometrically: the N–C–N angle and C–N bond lengths of the ligand can be assumed to be rigid, which leads, in the case of increasing M–N bond lengths (which is due to a larger effective ionic radius), to a decrease of the chelating angle (Scheme 2).

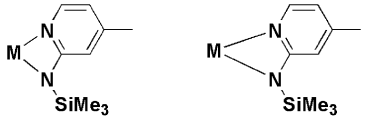

Scheme 2. Influence of M–N bond length on the N–M–N chelating angle. A short M–N distance leads to a relatively large chelating angle (left) and a large M–N distance leads to a small chelating angle (right).

The smallest angles are observed in the case of scandium, which has the largest effective ionic radius of the trivalent metals (mean angle: 62.11°). Titanium has a smaller effective ionic radius, which leads to a larger mean bond angle (64.07°). The largest N–M–N bond angles (mean angle: 65.98°) are found for chromium. It can therefore be concluded that the smaller the metal ion, the larger the N–M–N bond angle. The only metal ion that does not match this sequence perfectly is iron(III), possibly due to the large difference between the mean M–$N_{pyridine}$ and M–N_{amido} bond lengths (see Table 1).

$MnCl_2$, $CoCl_2$ and $FeCl_2$ were used as starting material to obtain manganese(II), cobalt(II) and iron(II) aminopyridinate. Two equivalents of 4-*tert*-butylpyridine (*t*BuPy) were employed as an additional neutral donor ligand in order to obtain an octahedral coordination sphere. After workup, [$Mn(Ap^{TMS})_2$(*t*BuPy)$_2$] (**3**) was obtained as a highly air-sensitive orange precipitate and [$Co(Ap^{TMS})_2$-(*t*BuPy)$_2$] (**4**) as an ochre-green precipitate, both in moderate yields. In the case of iron(II), [$Fe(Ap^{TMS})_2$(*t*BuPy)$_2$] (**5**) could be isolated as a dark red crystalline material in very good yields. Single crystals of **3**, **4** and **5** were obtained by concentration of the mother liquor followed by storage at –30 °C. The molecular structures of **3**, **4** and **5** were determined by X-ray analysis (Figures 3, 4 and 5, respectively). Further crystallographic details can be found in the Experimental Section.

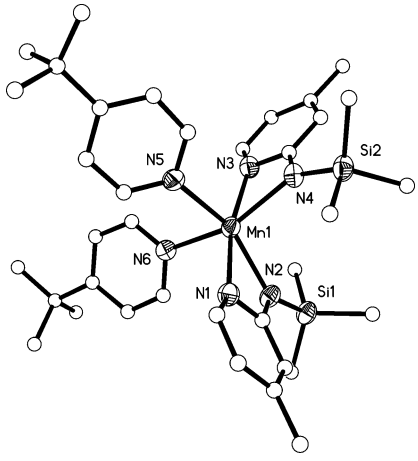

Figure 3. Molecular structure of **3** (ORTEP view; for clarity, only non-carbon atoms are drawn as 50% probability ellipsoids). Selected bond lengths [Å] and angles [°]: Mn1–N1 2.3077(16), Mn1–N2 1.1927(15), Mn1–N3 2.2997(16), Mn1–N4 2.1998(16), Mn1–N5 2.3240(15), Mn1–N6 2.3179(16); N1–Mn1–N2 60.20(5), N3–Mn1–N4 60.18(6), N5–Mn1–N6 87.99(6).

Complexes **3**, **4** and **5** are isostructural monomeric complexes containing two η^2-chelating ligands as well as two additional neutral *t*BuPy ligands in a *cis* arrangement. The N–M–N aminopyridinate bond angles vary from 59.86(15)° (N1–Co1–N2) to 62.02(9)° (N3–Fe1–N4) and reveal a

Table 1. Effective ionic radii and mean bond angles of homoleptic trivalent metal complexes.

Metal ion	Effective ionic radius	Mean N–M–N bond angle	Mean M–N distance	Mean M–$N_{pyridine}$ distance	Mean M–N_{amido} distance
Sc^{3+}	88.5	62.1	2.21	2.23	2.18
Ti^{3+} [4]	81	64.1	2.12	2.15	2.09
Fe^{3+}	78.5	64.0	2.11	2.17	2.04
Cr^{3+} [4]	75.5	66.0	2.06	2.04	2.07

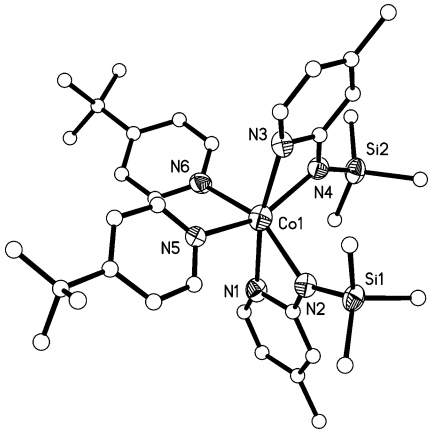

Figure 4. Molecular structure of **4** (ORTEP view; for clarity, only non-carbon atoms are drawn as 50% probability ellipsoids). Selected bond lengths [Å] and angles [°]: Co1–N1 2.310(5), Co1–N2 2.209(4), Co1–N3 2.284(5), Co1–N4 2.217(5), Co1–N5 2.328(5), Co1–N6 2.330(4); N1–Co1–N2 59.86(15), N3–Co1–N4 60.40(17), N5–Co1–N6 88.26(17).

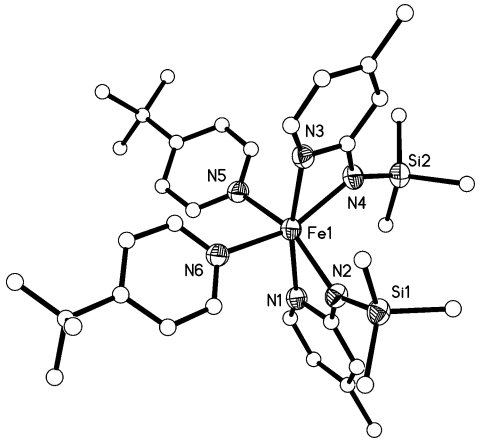

Figure 5. Molecular structure of **5** (ORTEP view; for clarity, only non-carbon atoms are drawn as 50% probability ellipsoids). Selected bond lengths [Å] and angles [°]: Fe1–N1 2.245(2), Fe1–N2 2.139(2), Fe1–N3 2.227(2), Fe1–N4 2.149(2), Fe1–N5 2.248(2), Fe1–N6 2.244(2); N1–Fe1–N2 61.90(8), N3–Fe1–N4 61.02(9), N5–Fe1–N6 87.54(8).

strained binding mode of the aminopyridinate ligands, which leads to a distorted octahedral coordination of the metal atom. The N_{amido}–M bond lengths are significantly shorter [2.1927(15) and 2.1998(16) Å for **3**; 2.209(4) and 2.217(5) Å for **4**; 2.139(2) and 2.149(2) Å for **5**] than the corresponding $N_{pyridine}$–M distances [2.2997(16) and 2.3240(16) Å for **3**; 2.284(5) and 2.310(5) Å for **4**; 2.227(2) and 2.245(2) Å for **5**], which indicates a localisation of the anionic function of the ligand at the amido N atom.

The *t*BuPy ligands are arranged in nearly ideal *cis* positions, with angles ranging from 87.54(8)° (N5–Fe1–N6) to 88.26(17)° (N5–Co1–N6). In the case of manganese, a structurally related aminopyridinate-cyclopentadienido complex exhibits similar Mn–N bond lengths (2.183–2.285 Å) and a similar N–Mn–N bond angle (60.52°).[24] The Co–N distances in complex **4** are similar to those in the only known cobalt aminopyridinate (1.998–2.355 Å) but the bite angle is smaller [59.86(15)° in comparison to 62.7° and 63.8°].[11]

Pure N_{amido}–Fe^{II} bonds usually vary from 1.892[35] to 2.085 Å[36] and are shorter than the bonds found in complex **5**, which suggests a mixture of both pure N_{amido}–Fe and pure $N_{pyridine}$–Fe bonds in this complex. The $N_{pyridine}$–Fe^{II} distances in **5** lie in the range of bond lengths found in the literature (1.992–2.307 Å).[37,38]

According to the trend described for the homoleptic trivalent metal aminopyridinates, a similar behaviour can be proposed for the series Mn^{2+}, Fe^{2+}, Co^{2+} and Ni^{2+}. The structurally analogous *cis* complexes should exhibit smaller chelating angles for larger metal ions, and this is indeed observed for magnanese(II), iron(II) and nickel(II)[12] complexes (see Table 2). The only exception is the cobalt complex, which shows an unexpectedly small N–M–N bond angle. This small angle is in accordance with the relatively long M–N bond length (compared to the other M^{2+} aminopyridinates).

Table 2. Effective ionic radii and mean bond angle of homoleptic trivalent metal complexes.

Metal ion	Effective ionic radius[39]	Mean N–M–N bond angle	Mean M–N distance
Mn^{2+}	97	60.2	2.25
Fe^{2+}	92	62.0	2.19
Co^{2+}	88.5	60.1	2.26
Ni^{2+} [12]	83	63.1	2.11

If the reaction with iron(II) is carried out without additional donor ligands, the yellow highly air-sensitive complex **6** is obtained in moderate yield. The molecular structure of **6** was determined by X-ray structure analysis (Figure 6). A highly symmetric trinuclear complex with a central (interstitial) five-coordinate oxygen atom bridging three iron and two lithium atoms is observed in the solid state.

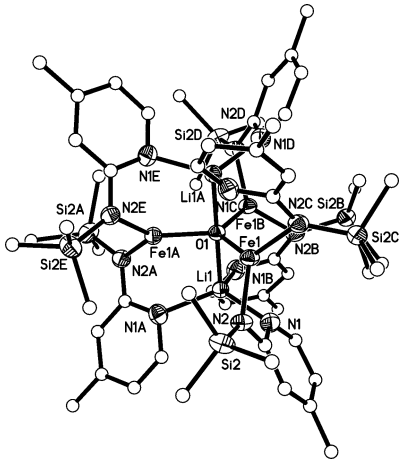

Figure 6. Molecular structure of **6** (ORTEP view; for clarity, only non-carbon atoms are drawn as 50% probability ellipsoids). Selected bond lengths [Å] and angles [°]: Fe1–O1 1.9504(7), Fe1–N2 2.021(3), Li1–O1 2.005(8), Li1–N1 2.094(4); O1–Fe1–N2 124.46(9), N2–Fe1–N2 111.08(18), N1–Li1–O1 102.2(2), N1–Li1–N1 115.65(16).

All iron atoms are coordinated by two N_{amido} nitrogen atoms from the Ap^{TMS} ligands and the central oxygen atom. The lithium atoms are coordinated tetrahedrally in a distorted fashion by three $N_{pyridine}$ donors and the central oxygen atom. The Fe–N distance [2.021(3) Å] lies in the range of known pure Fe^{II}–N_{amido} distances (1.892–2.307 Å).[35,36] Furthermore, the Li–N bond length is similar to those found in the literature (1.901–2.289 Å),[13,40] as are the Fe–O [1.9504(7) Å] and Li–O [2.005(8) Å] distances (literature: 1.840–2.100 Å[41,42] and 1.784–2.386 Å[43,44] for Fe–O and Li–O, respectively). The O1–Fe1–N2 bond angle is 124.46(9)° and the N2–Fe–N2 angle is 111.08(18)°, thereby revealing the trigonal coordination of the iron atom.

Zinc(II) was employed in a reaction with two equivalents of lithiated Ap^{TMS} to yield complex **7**. After workup, complex **7** was obtained as a white crystalline powder in moderate yields. The molecular structure of **7**, determined by X-ray analysis (Figure 7), shows that this complex is a dimer. A similar zinc aminopyridinate complex, in which two ligands bind to the metal in a strained η^2 coordination mode and the other two ligands bridge the zinc atoms, has been reported.[15] Interestingly, this latter complex exhibits an inversion centre in its solid-state structure, whereas complex **7** has C_2 symmetry. The two different coordination modes of the ligands would suggest that two separate signal sets should be observed for each ligand in the NMR experiments. However, in the case of **7** only one set of signals was observed in the ^1H, ^{13}C and ^{29}Si NMR spectra for all aminopyridinato ligands. These data are indicative of rapid ligand exchange processes. The Zn–N distances vary from 1.9752(19) (Zn1–N4) to 2.102(2) Å (Zn1–N1) and are similar to the Zn–N bond lengths of the known zinc aminopyridinate (1.943–2.127 Å), as are the N–Zn–N bond angles [65.43(8)° and 120.40(8)° in comparison to 65.12° and 123.14°].[15] The distance between the zinc atoms (3.270 Å) allows us to conclude that there is no interaction between the zinc atoms.

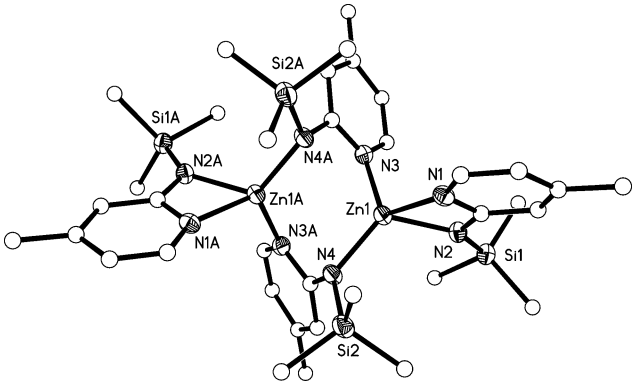

Figure 7. Molecular structure of **7** (ORTEP view; for clarity, only non-carbon atoms are drawn as 50% probability ellipsoids). Selected bond lengths [Å] and angles [°]: Zn1–N1 2.102(2), Zn1–N2 2.063(2), Zn1–N3 2.030(2), Zn1–N4 1.9752(19); N1–Zn1–N2 65.43(8), N3–Zn1–N4 120.40(8).

Magnetic Properties

Complexes **2** to **6** are paramagnetic. Measurements of the magnetic susceptibility were therefore carried out to characterise their magnetic behaviour. All measurements were performed at a field of 0.5 T.

Complex **2** is a high-spin iron(III) complex with a μ_{eff} value of 5.63 μ_B at 297 K. The effective magnetic moments of complexes **3** and **4** at 250 K are 5.88 and 4.80 μ_B, respectively. Both these complexes are also high-spin.

The high effective magnetic moment of complex **4** indicates a large spin-orbit coupling. The magnetic moment of complexes **3**, **4** and **5** remains stable upon lowering the temperature and shows only Curie paramagnetism. Complex **5** is a high spin iron(II) complex with an effective magnetic moment of 5.35 μ_B and does not show spin-crossover behaviour in the temperature range investigated (Figure 8). Complex **6** has an effective magnetic moment of 9.68 μ_B at room temperature, which indicates the existence of three separated iron(II) atoms with $S = 4/2$.

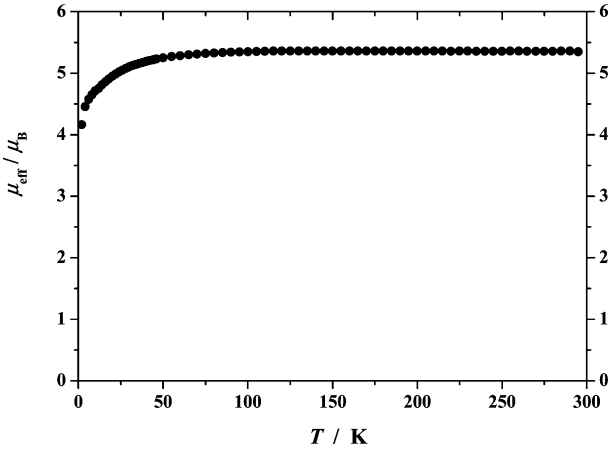

Figure 8. Dependency of the effective magnetic moment (μ_{eff}) of **5** on temperature at a field of 0.5 T.

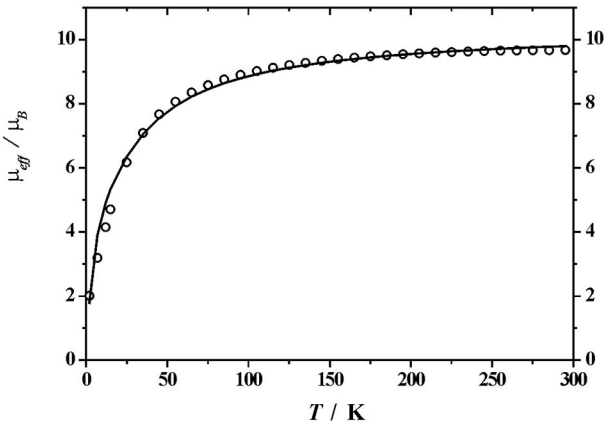

Figure 9. Dependency of the effective magnetic moment (μ_{eff}) of **6** on temperature at a field of 0.5 T (circles: experimental data; solid line: simulation).

This temperature-dependence is indicative of Curie law behaviour with a weak antiferromagnetic coupling between the iron centres, which lowers the effective magnetic moment to a remaining value of 2.01 μ_B at 2 K (Figure 9).The experimental data for trinuclear complex **6** were modelled by fitting to the appropriate Heisenberg–Dirac–van Vleck (HDvV) spin Hamiltonian for isotropic exchange coupling and Zeeman splitting [Equation (1)].[45]

$$\hat{H} = -2J\sum \hat{S}_i\hat{S}_j + g\mu_B B\sum \hat{S}_{iz} \quad (1)$$

A Curie–Weiss-type paramagnetic impurity (ρ) with spin $S = 4/2$ and temperature-independent paramagnetism (*TIP*) were included according to $\chi = (1 - \rho)\cdot\chi + \rho\cdot\chi_{mono} + TIP$.[46] The calculated curve fit is shown as a solid line in Figure 9. The best fit parameters are $g = 2.48$, $J = -2.7\ cm^{-1}$, $PI = 5.0\%$ (fixed) and $TIP = 2.0 \times 10^{-4}\ cm^3\,mol^{-1}$ (fixed).

Conclusions

We have presented the missing complexes of the first row transition metal aminopyridinates and have been able to show that one specific aminopyridinato ligand is able to stabilise all first row transition metal metals, which indicates the high versatility of this ligand and most likely of the ligand class. Homoleptic complexes were obtained for scandium(III) and iron(III), whereas manganese(II), iron(II) and cobalt(II) form structurally analogous *cis* complexes upon coordination of additional neutral ligands. All paramagnetic complexes are high-spin and show Curie paramagnetism.

If no additional neutral N ligands are added, iron(II) forms a highly symmetric trinuclear complex containing three weakly antiferromagnetically coupled high-spin metal centres. Zinc(II) yields a dimeric complex which exhibits C_2 symmetry.

Experimental Section

General: All reactions and manipulations with air-sensitive complexes were performed under dry argon, using standard Schlenk and glovebox techniques. Non-halogenated solvents were distilled from sodium benzophenone ketyl and halogenated solvents from P_2O_5. Deuterated solvents were obtained from Cambridge Isotope Laboratories and were degassed, dried with molecular sieves and distilled prior to use. All chemicals were purchased from commercial sources and used without further purification unless mentioned otherwise in the synthetic procedure. NMR spectra were recorded with either a Varian INOVA 300 or a Varian INOVA 400 spectrometer. Chemical shifts are reported in ppm relative to the deuterated solvent. Elemental analyses were carried out with a Vario elementar EL III. Magnetic data were measured with a Quantum-Design MPMS-5S SQUID magnetometer equipped with a 5-T magnet in the range 295–2 K. The powdered samples were contained in a gel bucket and fixed in a non-magnetic sample holder. Each raw data file for the measured magnetic moment was corrected for the diamagnetic contribution of the sample holder and the gel bucket. The molar susceptibility was corrected using Pascal constants and the increment method according to Haberditzl.[47]

Synthesis of 1: A solution of $Ap^{TMS}H$ (2.705 g, 15 mmol) in 80 mL of Et_2O was treated with 9.375 mL (1.6 M, 15 mmol) of *n*BuLi in hexanes at 0 °C and stirred for 30 min. After stirring overnight at room temperature the mixture turned from colourless to pale yellow. It was then added to a solution of $[ScCl_3(thf)_3]$ (1.838 g, 5 mmol) in 60 mL of thf at 0 °C. The colour remained pale yellow. The solution was again stirred overnight at room temperature. After removing the solvent, the residue was extracted with 60 mL of hexane, filtered and concentrated. Colourless crystals of **1** were obtained after storage in a freezer at –30 °C. Further concentration of the mother liquor yielded **1** as a white precipitate. Yield 1.065 g (1.8 mmol, 37%). $C_{27}H_{45}N_6ScSi_3$ (582.90): calcd. C 55.14, H 8.19, N 14.55; found C 55.63, H 7.78, N 14.42. ^{1}H NMR (C_6D_6, 296 K): δ = 0.37 (s, 27 H, TMS), 1.76 (s, 9 H, ar-CH_3), 5.82 (d, $J_{H,H}$ = 5.7 Hz, 3 H), 6.33 (s, 3 H), 7.55 (d, $J_{H,H}$ = 5.7 Hz, 3 H) ppm. ^{13}C NMR (C_6D_6, 296 K): δ = 1.66, 21.90, 110.85, 113.55, 143.72, 151.38, 170.68 ppm. ^{29}Si NMR (C_6D_6, 296 K): δ = –5.62 ppm.

Synthesis of 2: A solution of $Ap^{TMS}H$ (1.082 g, 6 mmol) in 15 mL of Et_2O was treated with 3.25 mL (1.6 M, 6 mmol) of *n*BuLi in hexanes at –50 °C and stirred for 30 min. After stirring overnight at room temperature the mixture turned from colourless to pale yellow. It was then added to a suspension of $FeCl_3$ (0.324 g, 2 mmol) in 15 mL of thf at –50 °C. The colour turned first red then dark purple. The solution was again stirred overnight at room temperature. After removing the solvent, the residue was extracted twice with 15 mL of hexane, filtered and concentrated. Dark purple crystals of **2** were obtained after storage at –30 °C. Further concentration of the mother liquor yielded **2** as a dark purple precipitate. Yield 0.707 g (1.2 mmol, 40%). $C_{27}H_{45}FeN_6Si_3$ (593.79): calcd. C 54.33, H 8.01, N 14.10; found C 54.61, H 7.64, N 14.15. μ_B = 5.44 (270 K, 0.5 T).

Synthesis of 3: A solution of $Ap^{TMS}H$ (3.606 g, 20 mmol) in 50 mL of Et_2O was treated with 12.5 mL (1.6 M, 20 mmol) of *n*BuLi in hexanes at 0 °C and stirred for 30 min. After stirring overnight at room temperature the mixture turned from colourless to pale yellow. It was then added to a suspension of $MnCl_2$ (1.258 g, 10 mmol) and *tert*-butylpyridine (2.9 mL, 20 mmol) in 100 mL of thf at 0 °C. The solution was again stirred overnight at room temperature and the colour changed to orange. After removing the solvent, the residue was extracted with 100 mL of hexane, filtered and concentrated. Light orange crystals of **3** were obtained after storage at –30 °C. Further concentration of the mother liquor yielded **3** as an orange precipitate. Yield 1.470 g (2.1 mmol, 22%). $C_{36}H_{56}MnN_6Si_2$ (683.98): calcd. C 62.97, H 8.32, N 12.35; found C 63.22, H 8.25, N 12.29. μ_B = 5.88 (250 K, 0.5 T).

Synthesis of 4: A solution of $Ap^{TMS}H$ (1.803 g, 10 mmol) in 50 mL of Et_2O was treated with 6.25 mL (1.6 M, 10 mmol) of *n*BuLi in hexanes at 0 °C and stirred for 30 min at that temperature and then overnight at room temperature. The mixture turned from colourless to pale yellow. It was then added to a suspension of $CoCl_2$ (0.650 g, 5 mmol) and *tert*-butylpyridine (1.47 mL, 10 mmol) in 20 mL of thf at 0 °C. The solution was again stirred overnight at room temperature, whereupon the coloured changed to dark green. After removing the solvent, the residue was extracted with 100 mL of hexane, filtered and concentrated. Ochre-green crystals of **4** were obtained after storage in a freezer at –30 °C. Further concentration of the mother liquor yielded **4** as an ochre-green precipitate. Yield 1.731 g (2.5 mmol, 50%). $C_{36}H_{56}CoN_6Si_2$ (687.97): calcd. C 62.42, H 8.15, N 12.59; found C 62.85, H 8.20, N 12.22. μ_B = 4.80 (250 K, 0.2 T).

Synthesis of 5: A solution of $Ap^{TMS}H$ (1.803 g, 10 mmol) in 50 mL of Et_2O was treated with 6.25 mL (1.6 M, 10 mmol) of *n*BuLi in hexanes at 0 °C and stirred overnight at room temperature. The

Table 3. Data of the X-ray crystal structure analyses.

Complex	**1**	**2**	**3**	**4**	**5**	**6**	**7**
Formula	$C_{27}H_{45}N_6ScSi_3$	$C_{27}H_{45}FeN_6Si_3$	$C_{36}H_{56}MnN_6Si_2$	$C_{36}H_{56}CoN_6Si_2$	$C_{36}H_{56}FeN_6Si_2$	$C_{54}H_{90}Fe_3Li_2N_{12}OSi_6$	$C_{36}H_{60}N_8Si_4Zn_2$
F_w	582.92	593.81	683.99	687.98	684.90	1273.35	848.02
Crystal system	triclinic	monoclinic	triclinic	triclinic	triclinic	trigonal	monoclinic
Space group	$P\bar{1}$	$P2_1/c$	$P\bar{1}$	$P\bar{1}$	$P\bar{1}$	$P6_322$	$C2/c$
a [Å]	9.6560(14)	17.6410(11)	11.5160(8)	11.5280(11)	11.4380(11)	16.1790(9)	24.5640(8)
b [Å]	11.2060(16)	12.1910(8)	13.2530(9)	13.2620(11)	13.1750(14)	16.1790(9)	9.4770(5)
c [Å]	16.006(2)	16.1570(11)	13.6260(9)	13.6540(13)	13.6440(14)	17.7250(10)	19.2960(11)
α [°]	101.535(11)	90	88.737(5)	88.632(7)	88.374(8)	90	90
β [°]	97.703(11)	104.601(5)	79.573(5)	79.496(8)	79.004(8)	90	92.175(5)
γ [°]	91.443(12)	90	73.192(5)	73.040(7)	73.192(8)	120	90
V [Å^3]	1679.2(4)	3362.5(4)	1956.9(2)	1962.3(3)	1931.3(3)	4018.1(4)	4488.7(4)
Z	2	4	2	2	2	2	4
T [K]	133(2)	191(2)	191(2)	191(2)	133(2)	133(2)	133(2)
d(calcd.) [g cm^{-3}]	1.153	1.173	1.161	1.164	1.178	1.052	1.255
μ [mm^{-1}]	0.351	0.580	0.430	0.530	0.484	0.661	1.209
2θ range [°]	3.72–51.07	2.60–51.99	3.04–52.22	3.03–51.75	3.04–52.00	2.90–51.90	3.32–52.25
ωR^2 (all data)	0.0853	0.0944	0.1140	0.1219	0.1052	0.1125	0.0678
R value	0.0526	0.0524	0.0408	0.0528	0.0473	0.0534	0.0319

mixture turned from colourless to pale yellow. It was then added to a suspension of $FeCl_2$ (0.630 g, 5 mmol) and *tert*-butylpyridine (1.47 mL, 10 mmol) in 50 mL of thf at 0 °C. The solution was again stirred overnight at room temperature and the colour changed to dark red-brown. After removing the solvent, the residue was extracted with 100 mL of hexane, filtered and concentrated. Dark red crystals of **5** were obtained after storage at –30 °C. Further concentration of the mother liquor yielded **5** as a dark red precipitate. Yield 2.720 g (4.0 mmol, 80%). $C_{36}H_{56}FeN_6Si_2$ (684.90): calcd. C 62.65, H 8.70, N 12.34; found C 63.13, H 8.24, N 12.27. μ_B = 5.35 (295 K, 0.5 T).

Synthesis of 6: A solution of $Ap^{TMS}H$ (1.443 g, 8 mmol) in 20 mL of Et_2O was treated with 5 mL (1.6 M, 8 mmol) of *n*BuLi in hexanes at 0 °C and stirred overnight at room temperature. The mixture turned from colourless to pale yellow. A suspension of $FeCl_2$ (0.507 g, 4 mmol) in 20 mL of thf was stirred overnight, then the solution of lithiated ligand was added at 0 °C and the mixture again stirred overnight at room temperature, whereupon the colour changed to very dark black-green. After removing the solvent, the residue was extracted with 50 mL of hexane, filtered and concentrated. Yellow-brown crystals of **6** were obtained after a few days at room temperature. Further concentration of the mother liquor yielded **1** as a yellow-brown precipitate. Yield 0.602 g (0.5 mmol, 35%). $C_{54}H_{90}Fe_3Li_2N_{12}OSi_6$ (1272.4): calcd. C 50.76, H 6.87, N 12.97; found C 50.93, H 7.13, N 13.21. μ_B = 9.68 (295 K, 0.5 T).

Synthesis of 7: A solution of $Ap^{TMS}H$ (3.606 g, 20 mmol) in 40 mL of Et_2O was treated with 12.5 mL (1.6 M, 20 mmol) of *n*BuLi in hexanes at 0 °C and stirred for 30 min. This mixture turned from colourless to pale yellow after stirring overnight at room temperature. It was then added to a solution of $ZnCl_2$ (1.363 g, 10 mmol) in 20 mL of thf at 0 °C. The colour remained pale yellow. The solution was again stirred overnight at room temperature. After removing the solvent, the residue was extracted with 40 mL of hexane, filtered and concentrated. Colourless crystals of **7** were obtained after storage in a freezer at –30 °C. Further concentration of the mother liquor yielded **7** as a white precipitate. Yield 1.215 g (1.4 mmol, 29%). $C_{36}H_{60}N_8Si_4Zn_2$ (848.04): calcd. C 51.18, H 7.55, N 12.99; found C 50.99, H 7.13, N 13.21. ^{1}H NMR (C_6D_6, 296 K): δ = 0.34 (s, 36 H, TMS), 1.81 (s, 12 H, ar-CH_3), 6.01 (d, $J_{H,H}$ = 4.2 Hz, 4 H), 6.52 (s, 4 H), 7.74 (d, $J_{H,H}$ = 4.2 Hz, 4 H) ppm. ^{13}C NMR (C_6D_6, 296 K): δ = 2.13, 21.55, 112.92, 115.70, 146.13, 150.40, 168.98 ppm. ^{29}Si NMR (C_6D_6, 296 K): δ = –2.09 ppm.

X-ray crystal structure analyses were performed with a STOE-IPDS II equipped with an Oxford Cryostream low-temperature unit. Structure solution and refinement were accomplished using SIR97,[48] SHELXL-97[49] and WinGX.[50] Crystallographic details are summarised in Table 3.

CCDC-706703 (for **1**), -706704 (for **2**), -706705 (for **3**), -706706 (for **4**), -706707 (for **5**), -706708 (for **6**) and -706709 (for **7**) contain the supplementary crystallographic data for this publication. These data can be obtained free of charge from The Cambridge Crystallographic Data Centre via www.ccdc.cam.ac.uk/data_request/cif.

Acknowledgments

Financial support from the Deutsche Forschungsgemeinschaft (DFG) (SPP 1181 "Nanoskalige anorganische Materialien durch molekulares Design") is gratefully acknowledged.

[1] R. Kempe, *Eur. J. Inorg. Chem.* **2003**, 791–803.
[2] R. Kempe, H. Noss, T. Irrgang, *J. Organomet. Chem.* **2002**, *647*, 12–20.
[3] R. Kempe, *Angew. Chem.* **2000**, *112*, 478–504; *Angew. Chem. Int. Ed.* **2000**, *39*, 468–493.
[4] A. Spannenberg, A. Tillack, P. Arndt, R. Kirmse, R. Kempe, *Polyhedron* **1998**, *17*, 845–850.
[5] E. Smolensky, M. Kapon, M. S. Eisen, *Organometallics* **2005**, *24*, 5495–5498.
[6] E. Smolensky, M. Kapon, J. D. Williams, M. S. Eisen, *Organometallics* **2005**, *24*, 3255–3265.
[7] R. Kempe, *Z. Kristallogr.* **1997**, *212*, 477.
[8] J. J. H. Edema, S. Gambarotta, A. Meetsma, A. L. Spek, N. Veldman, *Inorg. Chem.* **1991**, *30*, 2062–2066.
[9] F. A. Cotton, E. A. Hillard, C. A. Murillo, X. Wang, *Inorg. Chem.* **2003**, *42*, 6063–6070.
[10] F. A. Cotton, R. H. Niswander, J. C. Sekutowski, *Inorg. Chem.* **1978**, *17*, 3541–3545.
[11] H. K. Lee, C. H. Lam, S. L. Li, Z.-Y. Zhang, T. C. W. Mak, *Inorg. Chem.* **2001**, *40*, 4691–4695.
[12] S. Deeken, S. Proch, E. Casini, H. F. Braun, C. Mechtler, C. Marschner, G. Motz, R. Kempe, *Inorg. Chem.* **2006**, *45*, 1871–1879.
[13] L. M. Engelhardt, G. E. Jacobsen, W. Y. Patalinghug, B. W. Skelton, C. L. Raston, A. H. White, *J. Chem. Soc., Dalton Trans.* **1991**, 2859–2868.

[14] H. Aghabozorg, S. Gambarotta, C. Bensimon, *J. Sci. I. R. Iran* **1994**, *5*, 158–162.
[15] S. J. Birch, S. R. Boss, S. C. Cole, M. P. Coles, R. Haigh, P. B. Hitchcock, A. E. H. Wheatley, *Dalton Trans.* **2004**, 3568–3574.
[16] M. Jain, S. Mehra, P. C. Trivedi, R. V. Singh, *Met.-Based Drugs* **2002**, *9*, 53–60.
[17] S. Cabaleiro, J. Castro, J. A. García-Vázquez, J. Romero, A. Sousa, *Polyhedron* **2000**, *19*, 1607–1614.
[18] I. Beloso, J. Castro, J. A. García-Vázquez, P. Pérez-Lourido, J. Romero, A. Sousa, *Polyhedron* **2006**, *25*, 2673–2682.
[19] S. Cabaleiro, J. Castro, E. Vázquez-López, J. A. García-Vázquez, J. Romero, A. Sousa, *Polyhedron* **1999**, *18*, 1669–1674.
[20] H.-Y. Cheng, P.-H. Cheng, C.-F. Lee, S.-M. Peng, *Inorg. Chim. Acta* **1991**, *181*, 145–147.
[21] C.-F. Lee, S.-M. Peng, *J. Chin. Chem. Soc.* **1991**, *38*, 559–564.
[22] S. Cabaleiro, J. Castro, J. Romero, J. A. García-Vázquez, A. Sousa, *Acta Crystallogr., Sect. C* **2000**, *56*, 293–295.
[23] I. Beloso, J. Castro, J. A. García-Vázquez, P. Pérez-Lourido, J. Romero, A. Sousa, *Polyhedron* **2003**, *22*, 1099–1111.
[24] C. S. Alvarez, S. R. Boss, J. C. Burley, S. M. Humphry, R. A. Layfield, R. A. Kowenicki, M. McPartlin, J. M. Rawson, A. E. H. Wheatley, P. T. Wood, D. S. Wright, *Dalton Trans.* **2004**, 3481–3487.
[25] C. S. Alvarez, A. D. Bond, D. Cave, M. E. G. Mosquera, E. A. Harron, R. A. Layfield, M. McPartlin, J. M. Rawson, P. T. Wood, D. S. Wright, *Chem. Commun.* **2002**, 2980–2981.
[26] R. P. Davies, D. J. Linton, P. Schooler, R. Snaith, A. E. H. Wheatley, *Chem. Eur. J.* **2001**, *7*, 3696–3704.
[27] R. Kempe, P. Arndt, *Inorg. Chem.* **1996**, *35*, 2644–2649.
[28] L. E. Manzer, *Inorg. Synth.* **1982**, *21*, 135–140.
[29] S. Deeken, G. Motz, R. Kempe, *Z. Allg. Anorg. Chem.* **2007**, *633*, 320–325.
[30] C. Meermann, P. Sirsch, K. W. Tornroos, R. Anwander, *Dalton Trans.* **2006**, 1041–1050.
[31] M. E. G. Skinner, B. R. Tyrrell, B. D. Ward, P. Mountford, *J. Organomet. Chem.* **2002**, *647*, 145.150.
[32] M. B. Hursthouse, P. F. Rodesiler, *J. Chem. Soc., Dalton Trans.* **1972**, 2100–2102.
[33] Y. Ohgo, T. Ikeue, M. Nakamura, *Inorg. Chem.* **2002**, *41*, 1698–1700.
[34] W. Chiang, D. Vanegen, M. E. Thompson, *Polyhedron* **1996**, *15*, 2369–2376.
[35] T. Komuro, H. Kawaguchi, K. Tatsumi, *Inorg. Chem.* **2002**, *41*, 5083–5090.
[36] M. D. Fryzuk, D. B. Leznoff, E. S. F. Ma, S. J. Rettig, V. G. Young Jr., *Organometallics* **1998**, *17*, 2313–2323.
[37] C. R. Goldsmith, R. T. Jonas, A. P. Cole, T. D. P. Stack, *Inorg. Chem.* **2003**, *41*, 4642–4652.
[38] B. Weber, E. Kaps, *Heteroat. Chem.* **2005**, *16*, 391–397.
[39] R. D. Shannon, *Acta Crystallogr., Sect. A* **1976**, *32*, 751–767.
[40] S. M. Boss, J. M. Cole, R. Haigh, R. Snaith, A. E. W. Wheatley, *Organometallics* **2004**, *23*, 4527–4530.
[41] C.-C. Wu, S. A. Hunt, P. K. Gantzel, P. Gütlich, D. N. Hendrickson, *Inorg. Chem.* **1997**, *36*, 4717–4733.
[42] A. Abinati, F. Calderazzo, F. Marchetti, S. A. Mason, B. Melai, G. Pampaloni, S. Rizzato, *Inorg. Chem. Commun.* **2007**, *10*, 902–905.
[43] M. Veith, O. Schutt, V. Huch, *Angew. Chem. Int. Ed.* **2000**, *39*, 601–604; *Angew. Chem.* **2000**, *112*, 614–617.
[44] J. Gracia, A. Martin, M. Mena, M. del C. Morales-Varela, J.-M. Poblet, C. Santamaria, *Angew. Chem. Int. Ed.* **2003**, *42*, 927–930; *Angew. Chem.* **2003**, *115*, 957–960.
[45] O. Kahn, *Molecular Magnetism*, Wiley-VCH Publishers Inc., New York, **1993**.
[46] Simulation of the experimental magnetic data with a full-matrix diagonalisation of exchange coupling and Zeeman splitting was performed with the *julX* program developed by E. Bill (Max Planck Institute for Bioinorganic Chemistry, Mülheim/Ruhr, Germany).
[47] a) W. Haberditzl, *Angew. Chem.* **1966**, *78*, 277–312; *Angew. Chem. Int. Ed. Engl.* **1966**, *5*, 288–298; b) W. Haberditzl, *Magnetochemie*, Akademie-Verlag **1968**.
[48] A. Altomare, M. C. Burla, M. Camalli, G. L. Cascarano, C. Giacovazzo, A. Guagliardi, A. G. G. Moliterni, G. Polidori, R. Spagna, *J. Appl. Crystallogr.* **1999**, *32*, 115–119.
[49] G. M. Sheldrick, *SHELX-97*, Program for Crystal Structure Analysis (Release 97-2), Institut für Anorganische Chemie der Universität, Göttingen, Germany, **1998**.
[50] L. J. Farrugia, *J. Appl. Crystallogr.* **1999**, *32*, 837–838.

Received: November 10, 2008
Published Online: February 26, 2009

